9R.3

RADAR POLARIMETRY AT S, C, AND X BANDS COMPARATIVE ANALYSIS AND OPERATIONAL IMPLICATIONS

Alexander Ryzhkov[1] and Dusan Zrnic[2]

(1) CIMMS / University of Oklahoma, Norman, Oklahoma

(2) National Severe Storms Laboratory, Norman, Oklahoma

1. INTRODUCTION

Advantages of dual-polarization radar for rainfall estimation and radar echo classification have been proven in many research studies. Operational demonstration occurred during the Joint Polarization Experiment (JPOLE) using the polarimetric prototype of the WSR-88D radar (Ryzhkov et al. 2005). Based on the JPOLE results, the US National Weather Service plans to add soon polarimetric capability to all operational WSR-88D radars.

The JPOLE success also encouraged national services around the world to consider polarimetric upgrade of their radars operating either at the same frequency band (i.e., S band) or at shorter wavelength (e.g., C band). Other efforts are directed towards possible utilization of inexpensive X-band polarimetric radars to complement existing WSR-88D radars in the regions of poor coverage (as "gap fillers") or for monitoring rainfall over small areas. Therefore, adaptation of existing S-band polarimetric algorithms for precipitation estimation and radar echo classification for shorter wavelengths is an important practical issue.

At shorter wavelengths, effects of attenuation, resonance scattering, cross-coupling between orthogonal polarizations due to simultaneous transmission / reception become more significant compared to S band. Nonuniform beam filling has much larger impact on the quality of polarimetric measurements at shorter wavelengths, particularly for smaller radars with broader beams.

In this study, we address these problems by simulating realistic fields of polarimetric variables in rain at C and X bands based on the measured fields obtained from the dual-polarization WSR-88D radar. Polarimetric algorithms for radar echo classification and DSD retrieval are used for such simulation.

2. ATTENUATION AND RESONANCE EFFECTS

Here we briefly summarize the differences in radar scattering characteristics at S, C, and X bands in rain using theoretical simulations and large statistics of disdrometer measurements in central Oklahoma. The theoretical simulations are performed assuming that the aspect ratio of raindrops *a*/*b* depends on a drop equivolume diameter D according to the formula suggested by Brandes et al. (2002), the width of the canting angle distribution is 10º (Ryzhkov et al. 2002),

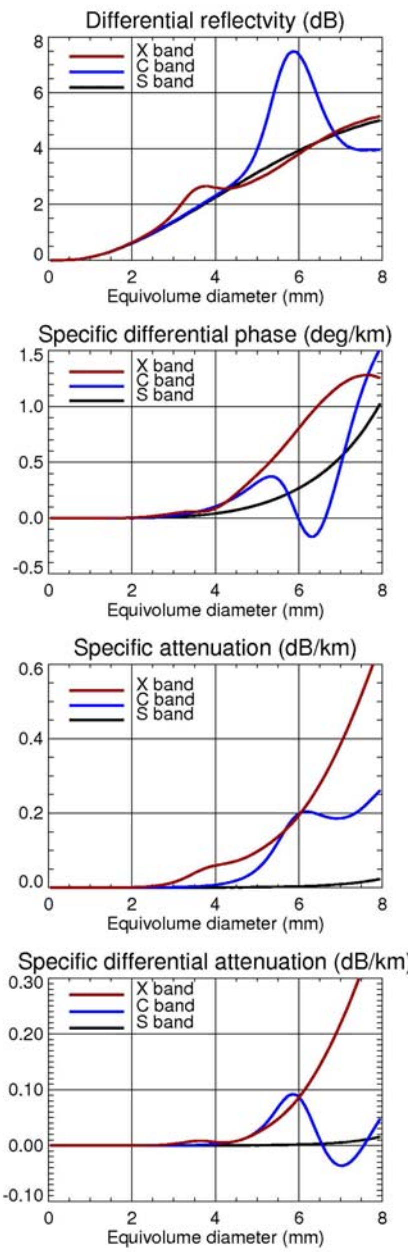

Fig. 1. Dependencies of Z_{DR}, K_{DP}, A_h, and A_{DP} on raindrop equivolume diameter at S, C, and X bands (T = 20ºC).

and temperature of raindrops is 20ºC.

Corresponding author address: Alexander Ryzhkov, CIMMS/NSSL, 1313 Halley Circle, Norman, OK, 73069, e-mail: Alexander.Ryzhkov@noaa.gov

Fig. 1 illustrates dependencies of differential reflectivity Z_{DR}, specific differential phase K_{DP}, specific attenuation A_h, and specific differential attenuation A_{DP} on equivolume diameter of individual raindrop at S band (λ = 11.0 cm), C band (λ = 5.45 cm), and X band (λ = 3.2 cm). It is evident that the resonance effects are less pronounced at X band compared to C band due to larger imaginary part of dielectric constant at X band (ε = 72.8 – j22.4 and 62.1 – j32.0 at C and X bands respectively). Indeed, the resonance effect is a result of interference of the electromagnetic waves reflected from the near and rear sides of the raindrop. If losses in the raindrop medium are high (as at X band) then the wave reflected from the rear side of the raindrop is significantly attenuated and interference is less pronounced. Because imaginary part of ε decreases with temperature, the resonance becomes stronger at higher temperatures of raindrop.

The resonance effects at C band can result in anomalously high Z_{DR}, negative K_{DP}, and negative A_{DP} that are not possible at S or X bands. Raindrops with sizes exceeding 5 mm are not very common in rain but their impact on most radar variables (especially Z_{DR}) is quite significant. We resort to the multi-year statistics of the 2D-video disdrometer measurements of drop size distributions (DSD) in Norman, OK to assess the impact of large drops on various radar variables at different radar frequencies. The dataset containing 27920 1-min DSD measurements was used in our estimation.

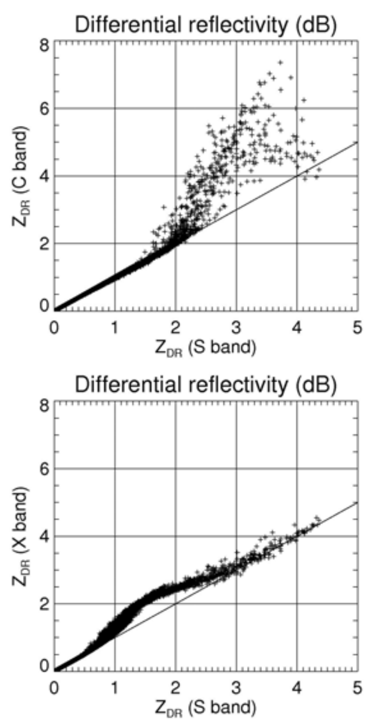

Fig. 2. Z_{DR} at C and X band versus Z_{DR} at S band as derived from disdrometer data.

Fig. 2 exhibits a scatterplots of differential reflectivities at S band (Z_{DR}(S)) versus differential reflectivities at C and X bands (Z_{DR}(C) and Z_{DR}(X)) computed from disdrometer data. It is clear that the difference between Z_{DR}(S) and Z_{DR}(C) becomes significant for Z_{DR}(S) > 2 dB, i.e., for DSD dominated by large drops. For such DSDs, the difference in Z_{DR} at S and X bands is small, but rain with Z_{DR}(S) between 1.0 and 2.5 dB exhibits noticeably higher Z_{DR}(X) than Z_{DR}(S).

The magnitude of the cross-correlation coefficient ρ_{hv} is also affected by the resonance effects at C band (Fig. 3). The cross-correlation coefficient might drop well below 0.98 at C band in pure rain, whereas the 0.98 ρ_{hv} threshold can be safely used as a cut-off value for rain at S and X band.

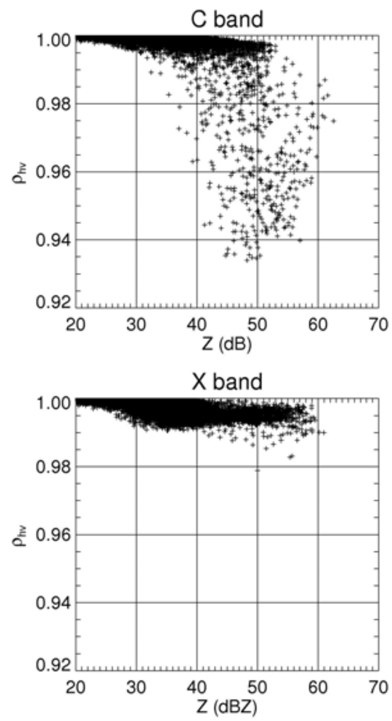

Fig. 3 Scatterplots of ρ_{hv} versus Z at C and X bands as derived from disdrometer data.

It is interesting that backscatter differential phase δ can be significantly larger at C than at X band for certain types of DSD that contain enough raindrops with sizes exceeding 5 mm (Fig. 4).

According to disdrometer data, DSDs with larger drops (i.e. with Z_{DR}(S) > 2.5 dB) constitute only 1 – 2% of all DSDs in the dataset but they are associated with about 10% of total rainfall. It is also known that the disdrometers (unlike radars) commonly underestimate the number of large drops in rain spectrum due to their relatively low concentrations and small size of the disdrometer sampling volume. Hence, the impact of large drops on radar measurements might be more significant than revealed from disdrometer data.

3. NONUNIFORM BEAM FILLING (NBF)

Nonuniform beam filling affects all radar variables but the largest impact is on measurements of differential phase and cross-correlation coefficient. Ryzhkov and Zrnic (1998), Gosset (2004), and Ryzhkov (2005)

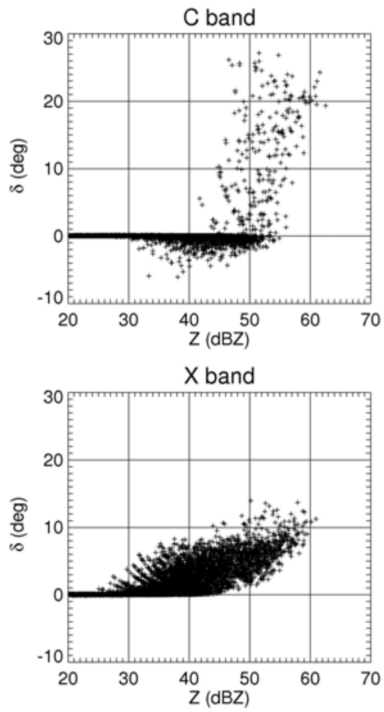

Fig. 4 Scatterplots of backscatter differential phase δ versus Z at C and X bands as derived from disdrometer data

demonstrated that variations of differential phase Φ_{DP} and radar reflectivity Z within the radar resolution volume may cause significant perturbations of the radial profile of Φ_{DP}.

The perturbation $\Delta\Phi_{DP}$ can be estimated using the following formula (Ryzhkov 2005):

$$\Delta\Phi_{DP} \approx 0.02\,\Omega^2\left(\frac{dZ_{HV}}{d\theta}\frac{d\Phi_{DP}}{d\theta} + \frac{dZ_{HV}}{d\varphi}\frac{d\Phi_{DP}}{d\varphi}\right) \quad , \quad (1)$$

where Ω is a one-way 3 dB antenna pattern width, and Z_{HV} is determined as 10 log $[\rho_{hv}\,(Z_h Z_v)^{1/2}]$ ($Z_{h,v}$ are radar reflectivity factors at horizontal and vertical polarizations expressed in linear scale). Eq (1) was derived assuming linear dependencies of Z_{HV} and Φ_{DP} on azimuthal and elevation angles θ and φ within the radar resolution volume and Gaussian shape of the radar antenna pattern.

NBF also reduces the magnitude of the cross-correlation coefficient ρ_{hv}. Such a reduction is described by the following expression (Ryzhkov 2005):

$$\rho_{hv}^{(b)} = \rho_{hv}\exp\{-0.045\,\Omega^2[\left(\frac{d\Phi_{DP}}{d\theta}\right)^2 + \left(\frac{d\Phi_{DP}}{d\varphi}\right)^2]\} \; . \quad (2)$$

Since differential phase and its gradients are directly proportional to the radar frequency, the impact of NBF is much more pronounced at C and X bands. Similarly, increasing an antenna beamwidth might result in significant increase of $\Delta\Phi_{DP}$ and the drop of ρ_{hv} in the presence of highly localized convection.

4. DSD RETRIEVAL

In order to compare polarimetric signatures in rain at different radar wavelengths we developed a simulator that takes the fields of polarimetric data collected with the KOUN WSR-88D radar and convert these into the fields of radar variables that should be expected at C and X bands. Such simulation implies DSD retrieval from the S-band polarimetric data. The DSD retrieval should be conducted only in the areas of rain, hence, the classification of radar echo is carried out prior to the retrieval. Classification is based on the principles of fuzzy logic as described by Schuur et al. (2003) and Ryzhkov et al. (2005).

We assume that DSD has a constrained Gamma form suggested by Zhang et al. (2001) and Brandes et al. (2004):

$$N(D) = N_0 D^{\mu} \exp(-\Lambda D) \quad , \quad (3)$$

where

$$\Lambda = 0.0365\,\mu^2 + 0.735\,\mu + 1.935 \quad . \quad (4)$$

According to Brandes et al. (2004), DSD is truncated at the drop size D_{max} that depends on Z:

$$D_{max} = 0.947 + 6.81\,10^{-3} Z + 4.25\,10^{-3} Z^2 - 1.12\,10^{-4} Z^3 + 1.25\,10^{-6} Z^4 + 1.0 \quad (5)$$

where Z is expressed in dBZ.

Our analysis shows that DSDs characterized by anomalously large Z_{DR} and moderate or low Z often observed in the radar data can not be matched with constrained Gamma DSD determined by Eq (3-5) regardless of the choice of μ. In such cases, we assume that the constrained Gamma DSD is truncated not only at higher end but also at lower end. In fact, quite often high values of Z_{DR} are attributed to the absence of small drops rather than to the presence of big drops. This is often the case in the updraft areas where small drops are suspended aloft and only few very big raindrops can fall through the updraft to the ground.

If Z_{DR} is too large (for a given Z) to fit any constrained Gamma DSD defined with (3) – (5), we assume that the DSD has a form determined by (3) and (4) but with fixed μ = -2 and it is truncated at D_{min} at lower end and at D_{max}+D_{min} (not exceeding 8 mm) at higher end. In other words, μ is fixed but a newly introduced parameter D_{min} is allowed to vary.

Following this methodology, we generated look-up tables of the DSD parameters μ, Λ, N_0, D_{min}, and D_{max} for any given pair of the measured Z and Z_{DR}.

5. EXAMPLE OF SIMULATION

After DSD parameters are determined, we can generate fields of all radar variables at S, C, and X bands using scattering computations as described in section 2. Nonuniform beam filling effects are accounted for by examining Z_{HV} and Φ_{DP} differences between adjacent radials separated by 1º in the horizontal and vertical directions.

As an example, we present results of simulations for rain event which occurred on May 13, 2004. Fields of Z and Z_{DR} at lowest elevation 0.5º in the area of interest are displayed in Fig. 5. The radar echo was classified as pure rain everywhere in the selected area. We focus our analysis on the region of convective rain in the northern part of the echo. This region is marked with high Z_{DR} observed at the periphery of convective cells. Figs. 6 – 8 illustrate radial profiles of different radar variables along the ray indicated in Fig. 5.

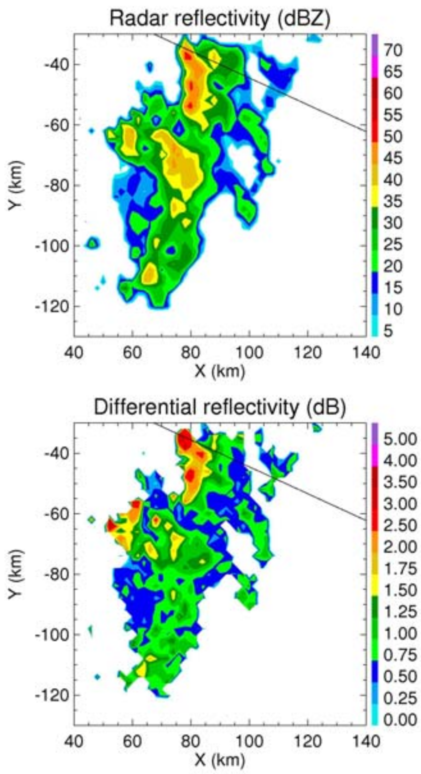

Fig. 5 Fields of Z and Z_{DR} measured by the KOUN WSR-88D radar on May 13, 2004 (1859 UTC) at elevation 0.5º.

As expected, radar reflectivities at C and X bands are affected by attenuation in the major convective cell centered at the distance 86.5 km from the radar (Fig. 6a). Radial profiles of Z_{DR} at C and X bands reflect combined effect of differential attenuation and the resonance (Fig. 6b). C-band Z_{DR} is much higher than S-band Z_{DR} in the main reflectivity core. Z_{DR}(C) becomes lower than Z_{DR}(S) behind the core where the effect of differential attenuation is dominant. Z_{DR}(X) is slightly higher than Z_{DR}(C) at 95 km due to the X-band resonance effect that offsets stronger differential attenuation at shorter wavelength.

Nonuniform beam filling (NBF) has almost negligible impact on Z and Z_{DR}. However, this is not the case for Φ_{DP} and ρ_{hv} . Differential phase exhibits nonmonotonic behavior as a function of range at all three radar frequencies (Fig. 7). The measured radial

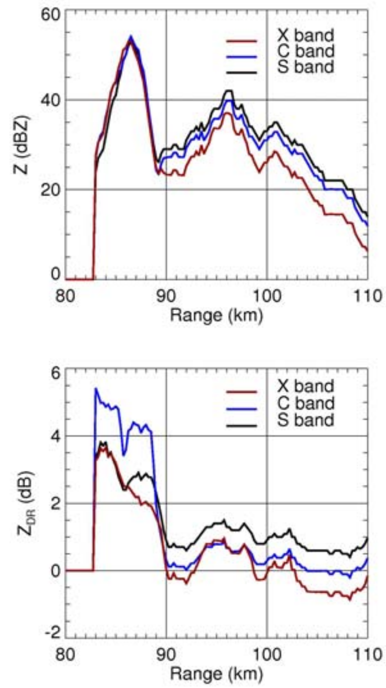

Fig. 6 Simulated radial profiles of Z and Z_{DR} at S,C, and X bands retrieved from the KOUN data at Az = 114º (Fig. 5).

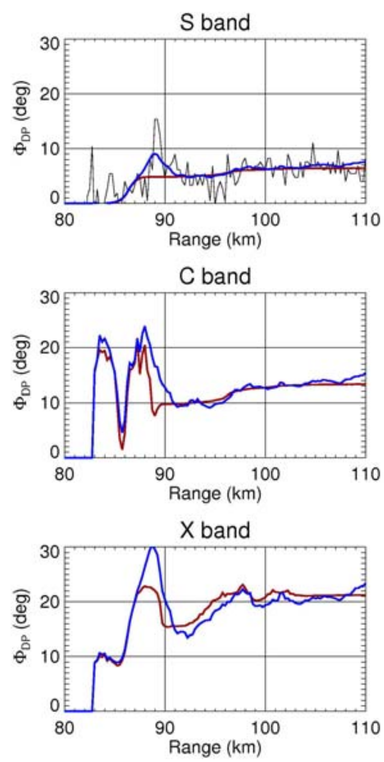

Fig. 7 Simulated radial profiles of Φ_{DP} at S, C, and X bands retrieved from the KOUN data at Az = 114º (Fig. 5). Blue lines – nonuniform beam filling (NBF) is accounted for; red lines – NBF is not accounted for. Black line in the top panel depicts Φ_{DP} measured by KOUN.

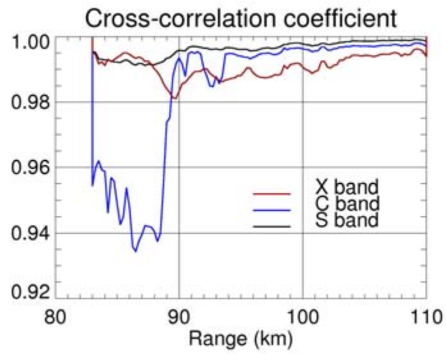

Fig. 8 Simulated radial profiles of ρ_{hv} at S, C, and X bands derived from the KOUN data at Az = 114° (Fig. 5).

profile of Φ_{DP} at S band (black line in Fig. 7a) is very well reproduced by the model Φ_{DP} (blue line). A bump in the Φ_{DP} profile at about 89 km is a result of NBF. Note the absence of the bump if the latter effect is not accounted for (red line). Good correspondence between the measured and model Φ_{DP} profiles at S band gives us more confidence in the model simulator.

Radial profile of Φ_{DP} at C band is dramatically different (Fig. 7b). There are two local maxima instead of one. Their primary origin is backscatter differential phase. The contribution from NBF is reflected in the difference between blue and red curves. The impact of NBF on Φ_{DP} is also substantial at X band (Fig. 7c).

The presence of large drops associated with high Z_{DR} in the main reflectivity core results in a substantial decrease of the cross-correlation coefficient ρ_{hv} at C band (Fig. 8). Such a decrease is primarily caused by the resonance effect.

6. DISCUSSION

Next we discuss modifications to the existing polarimetric algorithms for radar echo classification and rainfall estimation that are well explored and validated at S band.

6.1 *Attenuation correction*

Attenuation correction at C and X bands presents more serious challenge compared to S band where attenuation is only occasionally a problem. Existing methods for attenuation correction using differential phase Φ_{DP} stipulate that the ratios $\alpha = A_h/K_{DP}$ and $\beta = A_{DP}/K_{DP}$ are relatively independent of DSD and the biases of Z and Z_{DR} can be obtained from the following relations (Bringi et al. 1990):

$$\Delta Z = -\alpha \Phi_{DP} \qquad (6)$$

and

$$\Delta Z_{DR} = -\beta \Phi_{DP} \qquad (7)$$

In order to apply formulas (6) and (7) for attenuation correction at C and X bands, the δ part of Φ_{DP} should be identified and removed. This is hard to do because of (a) high noisiness of the differential phase in the parts of the storm where ρ_{hv} is relatively low and (b) additional oscillations of Φ_{DP} that are caused by nonuniform beam filling and have similar appearance as δ in the radial profiles of differential phase (see Fig. 7). Another problem is the dependence of the coefficients α and β in Eq (6) and (7) on temperature and mean raindrop shape as well as their high variability in the presence of large drops (i.e., for Z_{DR} > 2 dB).

The latter problem was first recognized by Carey et al. (2000). They recommend to identify the zones of large drops using estimates of ρ_{hv} and δ and utilize different (but fixed) coefficients α and β in these regions. This approach is not applicable everywhere because (a) it is very difficult to estimate δ reliably and (b) the coefficients α and β are highly variable in the regions of large drops for which the resonance effects can be significant, especially at C band (see Fig. 1).

An alternate approach for attenuation correction of Z was introduced by Testud et al. (2000) (ZPHI method). The ZPHI method aims at estimating radial profile of specific attenuation A_h with the difference between the starting and ending values of Φ_{DP} used as a constraint.

The ZPHI procedure also implies that the ratio $\alpha = A_h/K_{DP}$ is constant and fixed which is not the case in the areas of large drops. Bringi et al. (2001) proposed to generalize the ZPHI method by allowing the ratio α to vary. According to their approach, the appropriate value of α should be determined by matching the measured radial profile of Φ_{DP} and a "constructed" profile of Φ_{DP} computed as

$$\Phi_{DP}^{c}(r,\alpha) = \frac{2}{\alpha}\int_{r_0}^{r} A_h(s,\alpha)\,ds \qquad (8)$$

This scheme, however, may not work if radial profile of the measured Φ_{DP} is highly perturbed due to several factors discussed earlier.

Summarizing, we believe that although some studies report on successful attenuation correction at C and X bands (e.g., Carey et al. 2000; Le Bouar et al. 2001, Matrosov et al. 2002), the correction methods should be more carefully tested, particularly in the cases of strong isolated convection.

6.2 *Classification*

Differential reflectivity Z_{DR} and cross-correlation coefficient ρ_{hv} prove to be most useful polarimetric variables for classification of radar echo. One has to keep in mind that Z_{DR} in pure rain at C and X bands might be noticeably higher than the corresponding Z_{DR} at S band (Fig. 2). On the other hand, ρ_{hv} in rain at C band can drop dramatically if large drops are present (Fig. 3). As a result, the areas of large drops associated with updrafts or melting hail may be very efficiently identified with polarimetric measurements at C band. In any case, the parameters of membership functions in the fuzzy logic classification algorithm should be changed accordingly.

6.3 *Rainfall estimation*

To measure rainfall reliably, intrinsic (nonattenuated) Z and Z_{DR} should be estimated with the accuracy of 1 dB and 0.1 – 0.2 dB respectively. It is not obvious at the moment that the correction methods at C and X bands can provide an estimate of attenuation biases of Z and Z_{DR} with such a high precision. Therefore, the role of K_{DP} for rainfall estimation at shorter wavelengths might be even more important than at S band. However, as already mentioned, differential phase should be utilized with caution at shorter wavelengths because of possible contribution from δ, negative K_{DP} due to resonance effects, nonuniform beam filling, and large statistical fluctuations of Φ_{DP} and K_{DP} caused by lower ρ_{hv}. As our simulations show, these problems can be more serious at C band than at X band.

More rapid range degradation of the quality of polarimetric classification and rainfall estimation at shorter wavelengths is a natural consequence of stronger attenuation. We suspect, however, that in the cases of isolated convection it is not a loss of sensitivity due to attenuation but beamwidth effects that might restrict the use of polarimetric methods on short-wavelength radars (particularly with antenna beams wider than 1º).

6.4 *Cross-coupling*

Simultaneous transmission and reception of horizontally and vertically polarized waves is a preferable choice technique for dual-polarization weather radar (Doviak et al. 2000). One of the side effects of such a choice is cross-coupling between orthogonally polarized waves. Cross-coupling depends on depolarizing properties of propagation media. Preliminary results of our simulations show that it is negligible in rain at all three radar wavelengths examined.

Nevertheless, cross-coupling can be noticeable in such highly depolarizing media as hail and especially crystals in the upper parts of the thunderstorm clouds. We have clear evidence of that at S band. Because depolarization propagation effects are wavelength-dependent, one might expect more serious problems in nonrain medium at shorter wavelengths.

7. REFERENCES

Brandes, E., G. Zhang, and J. Vivekanandan, 2002: Experiments in rainfall estimation with a polarimetric radar in a subtropical environment. *J. Appl. Meteor.*, 41, 674 – 685.

Brandes, E., G. Zhang, and J. Vivekanandan, 2004: Comparison of polarimetric radar drop size distribution retrieval algorithms. *J. Atmos. Oceanic. Technol.*, **21**, 584 – 598.

Bringi, V., V. Chandrasekar, N. Balakrishnan, and D. Zrnic, 1990: An examination of propagation effects in rainfall on radar measurements at microwave frequencies. *J. Atmos. Oceanic Technol.*, **7**, 829 – 840.

Bringi, V., T. Keenan, and V. Chandrasekar, 2001: Correcting C-band radar reflectivity and differential reflectivity data for rain attenuation: a self-consistent method with constraints. *IEEE Trans. Geosci. Remote Sens.*, **39**, 1906 – 1915.

Carey, L.D., S.A. Rutledge, D.A. Ahijevich, and T.D. Keenan, 2000: Correcting propagation effects in C-band polarimetric radar observations of tropical convection using differential propagation phase. *J. Appl. Meteor.*, **39**, 1405 – 1433.

Gosset, M, 2004: Effect of nonuniform beam filling on the propagation of radar signals at X-band frequencies. Pt II. Examination of differential phase shift. *J . Atmos. Oceanic Technol.*, **21**, 358-367.

Doviak, R.J, V. Bringi, A.V. Ryzhkov, A. Zahrai, and D.S. Zrnic, 2000: Considerations for polarimetric upgrades to operational WSR-88D radars. *J. Atmos. Oceanic Technol.*, **17**, 257 – 278.

Le Bouar, E.,. J. Testud, and T. Keenan, 2001: Validation of the rain profiling algorithm "ZPHI" from the C-band polarimetric weather radar in Darwin. *J. Atmos. Oceanic Technol.,* **18**. 1819 – 1837.

Matrosov, S.Y., K.A. Clark, B.E. Martner, and A. Tokay, 2002: Measurements of rainfall with polarimetric X-band radar. *J. Appl. Meteor.*, **41**, 941 – 952.

Ryzhkov, A.V., and D.S. Zrnic, 1998: Beamwidth effects on the differential phase measurements of rain. *J . Atmos. Oceanic Technol.*, **15**, 624-634.

Ryzhkov, A.V., D.S. Zrnic, J.C. Hubbert, V.N. Bringi, J. Vivekanandan, E.A. Brandes, 2002: Polarimetric radar observations and interpretation of co-cross-polar correlation coefficients. *J. Atmos. Oceanic Technol*, **19**, 340 - 354.

Ryzhkov, A.V., T.J. Schuur, D.W. Burgess, P.L. Heinselman, S.E. Giangrande, and D.S. Zrnic, 2005: The Joint Polarization Experiment. Polarimetric rainfall measurements and hydrometeor classification. *Bull. Amer. Meteor. Soc.*, **86,** 809-824.

Ryzhkov, A.V., 2005: On the use of differential phase for polarimetric rainfall measurements. A new approach to K_{DP} estimation. *This volume*.

Schuur T., A. Ryzhkov, P. Heinselman, D. Zrnic, D. Burgess, and K. Scharfenberg, 2003: Observations and classification of echoes with the polarimetric WSR-88D radar. National Severe Storms Laboratory Rep., 46 pp. Available online at http://www.nssl.noaa.gov/88d-upgrades/WSR-88D_reports.html.

Testud, J., E. Le Bouar, E. Obligis, and M. Ali-Mehenni, 2000: The rain profiling algorithm applied to polarimetric weather radar. *J. Atmos. Oceanic Technol.,* **17**, 332 – 356.

Zhang, G., J. Vivekanandan, and E. Brandes, 2001: A method for estimating rain rate and drop size distribution from polarimetric radar measurements. *IEEE Trans. Geosci. Remote Sens.*, **39**, 830-841.